

ULTRAHIGH-ENERGY NEUTRINO INTERACTIONS AND NEUTRINO TELESCOPE EVENT RATES *

Raj Gandhi,¹ Chris Quigg,² M. H. Reno,³ and Ina Sarcevic⁴

¹Mehta Research Institute,
10, Kasturba Gandhi Marg, Allahabad 211002, India

²Fermi National Accelerator Laboratory,
Batavia, IL 60510 USA

³Department of Physics and Astronomy,
University of Iowa, Iowa City, IA 52242 USA

⁴Department of Physics,
University of Arizona, Tucson, AZ 85721 USA

ABSTRACT

We present results for neutrino-nucleon cross sections for energies up to 10^{21} eV, of relevance to the detection of ultrahigh energy galactic and extragalactic neutrinos. At the highest energies, our results are about 2.4 times larger than previous estimates. Using these new cross sections, we predict neutrino telescope event rates for the upward moving muons initiated by the neutrino interactions in the Earth and for the contained-vertex events in the PeV range due to neutrino-electron interactions. We show that future neutrino detectors, such as AMANDA, BAIKAL, DUMAND and NESTOR have a very good chance of detecting neutrinos which originate in the Active Galactic Nuclei.

INTRODUCTION

The Active Galactic Nuclei (AGN), with typical luminosities in the range 10^{42} to 10^{48} erg/s, are believed to be the most powerful individual sources of radiation in the Universe. These extragalactic point sources are also considered as prodigious particle accelerators presumably powered by the gravitational energy of matter spiraling in to a supermassive black hole, though the mechanism responsible for the conversion of gravitational energy to luminous energy is not presently understood. Recent detection of energetic photons ($E_\gamma \sim 100$ MeV) from about 40 AGNs by the EGRET collaboration¹ and of TeV photons from Mkn 421, Mkn 501² and most recently from 1ES2344+514

*Talk presented by I. Sarcevic at *International Conference on Neutrino Mass, Dark Matter and Gravitational Waves*, Miami Beach, Florida, January 25 - 28, 1996.

by the Whipple collaboration³ have created new excitement in the field of high-energy gamma-ray physics. If the observed photons are decay products of π^0 s produced in hadronic interactions in the disk surrounding the AGN, then AGNs are also powerful sources of ultrahigh-energy (UHE) neutrinos.⁴ Unlike photons, which are absorbed by a few hundred gm/cm^2 of material, TeV neutrinos have interaction lengths on the order of $250 \text{ kt}/\text{cm}^2$ and thus can provide a direct window to the most energetic processes in the universe.

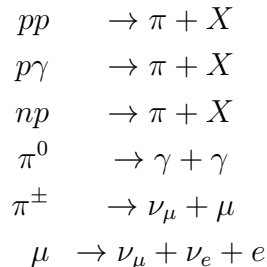
The advantage of the long interaction length translates to a challenge in the detection of neutrinos. Interaction rates increase with energy, but the fluxes of UHE neutrinos are steeply falling functions of neutrino energy. Cerenkov detection of muons from interactions of muon neutrinos in the rock or ice surrounding the detector is feasible.⁵ More difficult is the detection of charged-current interactions of electron neutrinos. Large-area air shower arrays or large volume underground detectors may be adequate for the detection of electron neutrinos, especially near the W -boson resonance in $\bar{\nu}_e e$ collisions. Theoretical calculations of the neutrino-nucleon and neutrino-electron cross sections are instrumental in evaluating event rates for neutrino telescopes.

Here we present results⁶ for charged current and neutral current cross sections for energies up to 10^{21} eV obtained using new parton distributions measured in ep collisions at HERA.⁷ We also discuss how detection of UHE neutrinos depends on these cross sections and on the neutrino fluxes from UHE neutrino sources. Event rates for muon neutrino conversions to muons are compared with earlier results based on older parton distribution functions.⁸ We also present results for contained events with higher threshold energies.

SOURCES OF UHE NEUTRINOS

A variety of sources may contribute to the neutrino flux at the surface of the Earth. Three types of sources are discussed here: atmospheric neutrinos from cosmic-ray interactions in the atmosphere, neutrinos from active galactic nuclei, and cosmic neutrinos from extragalactic cosmic ray interactions with the microwave background radiation. Model predictions for neutrino fluxes from these three types of sources are shown in Figure 1. Atmospheric neutrinos⁹ (ATM), while interesting in their own right, mask extraterrestrial sources for $E_\nu < 1$ TeV. Consequently, we restrict our discussion to neutrino energies above 1 TeV.

The TeV photons observed by Whipple collaboration² may be byproducts of hadronic cascades initiated by the protons generated within the AGN accretion disk of gas, or in the jets, which interact with matter or radiation in the AGN disk, to produce pions whose decay products include both photons and neutrinos. The structure of the corresponding hadronic cascade is:



If charged and neutral pions are produced in equal proportions and photons originate in hadronic cascades, simple counting leads to equal fluxes of photons and $\nu_\mu + \bar{\nu}_\mu$. The flux of $\nu_e + \bar{\nu}_e$ equals half of the flux of $\nu_\mu + \bar{\nu}_\mu$. The observed photon energy spectrum

Figure 1: Muon neutrino plus antineutrino fluxes at the Earth’s surface: angle-averaged flux from atmospheric neutrinos (ATM), diffuse flux from active galactic nuclei (AGN-NMB, AGN-SP and AGN-SS) and cosmic neutrinos (CR-2 and CR-4). The Fréjus upper limit¹⁴ on a neutrino flux in excess of atmospheric neutrino flux is indicated at 2.6 TeV. The dotted line indicates the vertical flux of atmospheric $\mu + \bar{\mu}$ from Ref. 15.

is a power-law with²

$$\frac{dN_\gamma}{dE_\gamma} \sim E_\gamma^{-2}$$

for $100 \text{ MeV} \leq E_\gamma \leq 2 \text{ TeV}$, and the same for neutrinos. We have chosen three representative fluxes of neutrinos from AGN, each corresponding to the diffuse flux integrated over all AGNs. These fluxes are shown in Figure 1. The Nellen, Mannheim and Biermann flux¹⁰ (AGN-NMB), which comes from assuming that pp collisions are the dominant neutrino source, is parameterized by:

$$\frac{dN_{\nu_\mu + \bar{\nu}_\mu}}{dE_\nu} = 1.13 \times 10^{-12} (E_\nu / \text{TeV})^{-2} \text{cm}^{-2} \text{s}^{-1} \text{sr}^{-1} \text{GeV}^{-1}$$

with the $\nu_e + \bar{\nu}_e$ spectrum assumed to be 1/2 of $\nu_\mu + \bar{\nu}_\mu$. The neutrino luminosity of a source is normalized to the observed diffuse x-rays and γ -rays. The NMB parameterization is valid for $E_\nu \leq 4 \times 10^4 \text{ GeV}$. In our calculations described in the next section, we have used this parameterization up to $E_\nu = 10^8 \text{ GeV}$. A somewhat different assumption of the luminosity is used by Szabo and Protheroe¹¹ (AGN-SP) in their extended model of neutrino sources, yielding a higher normalization of dN/dE_ν at 1 TeV. Above $E_\nu > 10^6 \text{ GeV}$, the AGN-SP follows a steeper power law,

$$dN/dE_\nu \sim E^{-3.5}$$

which accounts for the lack of protons at even higher energies required to produce neutrinos. The Stecker and Salamon flux¹² (AGN-SS) contains contributions from both pp and $p\gamma$ interactions in the accretion disk and has a nearly constant value of dN/dE_ν up to $E_\nu \sim 10^5 \text{ GeV}$.

Two models of neutrino fluxes from cosmic ray interactions with the microwave background¹³ are labeled CR-2 and CR-4 in Figure 1. The fluxes depend on the redshift of the cosmic ray sources. Maximum redshifts contributing are $z_{max} = 2$ and $z_{max} = 4$, respectively.

The electron neutrino plus antineutrino fluxes, to a good approximation, are equal to half of the fluxes shown in Figure 1.

UHE MUON NEUTRINOS

The primary means of detection of muon neutrinos and antineutrinos is by charged-current conversion into muons and antimuons. The long range of the muon means that the effective volume of an underground detector can be significantly larger than the instrumented volume. For example, a 10 TeV muon produced by a charged-current interaction in rock will propagate several kilometers in water-equivalent distance units before its energy is degraded to 1 TeV.

Backgrounds to AGN sources of $\nu_\mu + \bar{\nu}_\mu$ include atmospheric neutrinos and atmospheric muons. Muons produced by cosmic ray interactions in the atmosphere mask astrophysical signals unless detectors are very deep underground, muon energy thresholds are set very high, or one observes upward-going muons. We evaluate here event rates for upward-going muons produced in the rock surrounding the detector, for muon energy thresholds above 1 TeV and 10 TeV.

The neutrino-nucleon cross section comes into the calculation of the event rate in two ways. The probability of conversion $\nu_\mu \rightarrow \mu$ is proportional to the νN charged current cross section. In addition, the neutrino flux is attenuated by passage through the Earth. In the next section we describe our calculation of the neutrino-isoscalar nucleon (νN) cross section. The νN charged-current reaction is the dominant source of neutrino interactions except in a very narrow energy window at the W -boson resonance.

SMALL- x PARTON DISTRIBUTION FUNCTIONS AND $\sigma(\nu N)$

The inclusive cross section for $\nu_\mu + N \rightarrow \mu^- + X$ is given by

$$\frac{d^2\sigma}{dx dy} = \frac{2G_F^2 M E_\nu}{\pi} \frac{M_W^4}{(Q^2 + M_W^2)^2} [xq(x, Q^2) + x(1-y)^2 \bar{q}(x, Q^2)], \quad (1)$$

where $x = Q^2/2M\nu$, $y = \nu/E_\nu$, with $-Q^2$ the momentum transfer between the neutrino and muon, and ν the lepton energy loss in the lab frame, $\nu = E_\nu - E_\mu$. M is the mass of the nucleon and M_W is the mass of the W -boson, while the Fermi constant is $G_F = 1.16 \times 10^{-5} \text{ GeV}^{-2}$. Taking the target as isoscalar nucleons, in terms of the parton distribution functions for the proton,

$$q(x, Q^2) = \frac{u_v + d_v}{2} + \frac{u_s + d_s}{2} + s_s + b_s \quad (2)$$

$$\bar{q}(x, Q^2) = \frac{u_s + d_s}{2} + c_s + t_s \quad (3)$$

where we have written explicitly valence (v) and sea (s) distributions.

The general form of the cross section shows that at low energies, where the four-Fermi approximation is valid, $\sigma \sim E$. At higher energies, the W -boson propagator plays an important role. The value of $\langle Q^2 \rangle$ saturates at $\sim M_W^2$, and $x \sim M_W^2/(2ME_\nu y)$ decreases. For neutrino energies above 10^5 GeV , the small- x ($x \leq 3 \times 10^{-2}$) behavior of the parton distribution functions becomes important for the evaluation of the cross section.

Figure 2: Comparison of the light-quark sea at $Q^2 = M_W^2$ for various parton distribution functions. Of the MRS distributions, D₋ (A') is the most (least) singular.

Figure 3: The charged-current cross section for the CTEQ-DIS, CTEQ-DLA, EHLQ-DLA, MRS A', MRS G and MRS D₋ parton distribution functions. The data point, an average of ZEUS and H1, is from Ref. 17.

Neutrino charged-current interactions have been measured directly in laboratory experiments for neutrino energies up to $E_\nu = 300$ GeV.¹⁶ Charged-current ep scattering at HERA, equivalent to $E_\nu = 47.4$ TeV, can be translated to a value of $\sigma(\nu N)$.¹⁷ Recent ZEUS and H1 measurements at HERA⁷ of F_2^{ep} at small- x ($10^{-4} \leq x \leq 10^{-2}$) and for a large range of Q^2 , $4 \text{ GeV}^2 \leq Q^2 \leq 1600 \text{ GeV}^2$ have provided valuable information about parton densities at small- x and low- Q^2 . To evaluate the neutrino-nucleon cross section at ultrahigh energies, extrapolations beyond the measured regime in x and Q^2 are required.

There are two main theoretical approaches in the evolution in Q^2 of parton densities: Gribov-Lipatov-Altarelli-Parisi¹⁸ (GLAP) evolution and Balitskii-Fadin-Kuraev-Lipatov¹⁹ (BFKL) evolution. In the GLAP approach, parton distribution functions are extracted at modest values of Q^2 and evolved to higher scales. The BFKL approach involves a leading $\alpha_s \ln(1/x)$ resummation of soft gluon emissions, which generates a singular behavior in x at an initial scale Q_0 ,

$$xq_s(x, Q_0^2) \sim x^{-0.5} \quad (4)$$

for small x , which persists at higher values of Q . In our extrapolation of the parton distribution functions outside the measured region, we use GLAP evolution with input at $Q_0 = 1.6$ GeV,

$$xq_s(x, Q_0^2) \sim x^{-\lambda}. \quad (5)$$

The value of λ is determined by fits to deep-inelastic scattering and hadron-hadron data by the MRS²⁰ and CTEQ²¹ Collaborations. The MRS set A' has $\lambda = 0.17$, the MRS set G has $\lambda = 0.07$ while the MRS set D₋ has $\lambda = 0.5$. All of the MRS distribution functions are fitted using the $\overline{\text{MS}}$ factorization scheme. The CTEQ-DIS, using the deep-inelastic scattering factorization scheme, has $\lambda = 0.33$. These distribution functions are extrapolated using the power law fit to the distribution functions at $x = 10^{-5}$ and $Q = M_W$. We have also extrapolated the leading-order CTEQ distributions using the double-log approximation.²² For reference, the Eichten *et al.*²³ parton distribution functions, extrapolated using the double-log approximation, are also shown. The spread in values for the parton distribution functions is an indication of the uncertainty in evaluating the νN cross section.

For each of these sets of distribution functions, we have evaluated the neutrino-nucleon cross section. Figure 3 illustrates the range of predictions as a function of neutrino energy. Also shown is the average of H1 and ZEUS effective neutrino nucleon cross sections.¹⁷ There is excellent agreement among the predictions of the MRS D₋, G, and A' distributions and the CTEQ3 distributions up to $E_\nu \approx 10^7$ GeV. Above that energy, our DLA modification of the CTEQ3 distributions gives a lower cross section than the full CTEQ3 distributions (CTEQ-DIS), as expected from its less singular behavior as $x \rightarrow 0$. At the highest energy displayed, the most singular (MRS D₋) distribution predicts a significantly higher cross section than the others. Above about 10^6 GeV, the EHLQ-DLA distributions yield noticeably smaller cross sections than the modern distributions. Plots similar to Figure 3 for antineutrino-nucleon charged current interactions, as well as neutral current interactions, can be found in Ref. 6. For charged current and neutral current interactions, for $10^{15} \text{ eV} \leq E_\nu \leq 10^{21} \text{ eV}$, the cross sections follow a simple power law, for example

$$\sigma_{CC}(\nu N) = 2.69 \times 10^{-36} \text{ cm}^2 \left(\frac{E_\nu}{1 \text{ GeV}} \right)^{0.402}.$$

Table 1: Number of upward $\mu + \bar{\mu}$ per year per steradian for $A = 0.1 \text{ km}^2$ and $E_\mu^{\text{min}} = 1 \text{ TeV}$.

Fluxes	EHLQ-DLA	CTEQ-DIS
AGN-SS ¹²	82	92
AGN-NMB ¹⁰	100	111
AGN-SP ¹¹	2660	2960
ATM ⁹	126	141

Table 2: As in Table 1, but for $E_\mu^{\text{min}} = 10 \text{ TeV}$.

Fluxes	EHLQ-DLA	CTEQ-DIS
AGN-SS ¹²	46	51
AGN-NMB ¹⁰	31	34
AGN-SP ¹¹	760	843
ATM ⁹	3	3

NEUTRINO TELESCOPE EVENT RATE

In order to calculate the number of upward-moving muons that can be detected with neutrino detectors such as AMANDA, BAIKAL, DUMAND II and NESTOR,⁵ we fold in the neutrino flux and its attenuation in the Earth with the probability that a neutrino passing on a detector trajectory creates a muon in the rock that traverses the detector.

The attenuation of neutrinos in the Earth is described by a shadow factor $S(E_\nu)$, equivalent to the effective solid angle for upward muons, normalized to 2π :

$$\frac{dS(E_\nu)}{d\Omega} = \frac{1}{2\pi} \exp\left(-z(\theta)N_A\sigma_{\nu N}(E_\nu)\right), \quad (6)$$

where $N_A = 6.022 \times 10^{23} \text{ mol}^{-1} = 6.022 \times 10^{23} \text{ cm}^{-3}$ (water equivalent) is Avogadro's number, and $z(\theta)$ is the column depth of the earth, in water-equivalent units, which depends on zenith angle.²⁵ The probability that the neutrino with energy E_ν converts to a muon is proportional to the cross section and depends on the threshold energy for the muon E_μ^{min} :

$$P_\mu(E_\nu, E_\mu^{\text{min}}) = \sigma_{CC}(E_\nu)N_A\langle R(E_\nu, E_\mu^{\text{min}}) \rangle, \quad (7)$$

where the average muon range in rock is $\langle R \rangle$.²⁶ A more detailed discussion appears in Ref. 6.

The diffuse flux of AGN neutrinos, summed over all AGN sources, is isotropic, so the event rate is

$$\text{Rate} = A \int dE_\nu P_\mu(E_\nu, E_\mu^{\text{min}}) S(E_\nu) \frac{dN_\nu}{dE_\nu}, \quad (8)$$

given a neutrino spectrum dN_ν/dE_ν and detector area A . As the cross section increases, P_μ increases, but the effective solid angle decreases.

Event rates for upward muons and antimuons for a detector with $A = 0.1 \text{ km}^2$ for $E_\mu^{\text{min}} = 1 \text{ TeV}$ and $E_\mu^{\text{min}} = 10 \text{ TeV}$ are shown in Tables 1 and 2. The CTEQ-DIS distribution functions are taken as representative of the modern parton distribution

Table 3: Downward resonance $\bar{\nu}_e e \rightarrow W^-$ events per year per steradian for a detector with effective volume $V_{\text{eff}} = 1 \text{ km}^3$ together with the potential downward (upward) background from ν_μ and $\bar{\nu}_\mu$ interactions above 3 PeV.

Mode	AGN-SS ¹²	AGN-SP ¹¹
$W \rightarrow \bar{\nu}_\mu \mu$	6	3
$W \rightarrow \text{hadrons}$	41	19
$(\nu_\mu, \bar{\nu}_\mu)N \text{ CC}$	33 (7)	19 (4)
$(\nu_\mu, \bar{\nu}_\mu)N \text{ NC}$	13 (3)	7 (1)

function sets, and compared with the EHLQ-DLA event rate predictions. The muon range is that of Ref. 26.

The theoretical predictions for ultrahigh-energy neutrinos from AGNs yield event rates comparable to, or in excess of, the background rate of atmospheric neutrinos for $E_\mu^{\text{min}} = 1 \text{ TeV}$. The AGN-SP rate is large compared to the AGN-NMB rate because additional mechanisms are included. Flux limits from the Fréjus experiment are inconsistent with the SP flux for $1 \text{ TeV} < E_\nu < 10 \text{ TeV}$.¹⁴ The atmospheric neutrino background is greatly reduced by requiring a 10 TeV muon threshold, though AGN induced event rates are reduced as well. The flatter neutrino spectra have larger contributions to the event rate for muon energies away from the threshold muon energy than the steep atmospheric flux.

We have evaluated the event rates using the other parton distribution functions shown in Figure 2. Event rate predictions are unchanged with the other modern parton distributions because all these distributions are in agreement in the energy range $E_\nu \sim 1 - 100 \text{ TeV}$. However, our results for event rates are about 15% larger than for the EHLQ structure functions. This is due to the fact that EHLQ parton distributions were based on the CERN-Dortmund-Heidelberg-Saclay measurements of neutrino-nucleon structure functions¹⁶ which had low normalization of about 15%.

UHE ELECTRON NEUTRINOS

Finally we consider event rates from electron neutrino and antineutrino interactions. For $\nu_e N$ (and $\bar{\nu}_e N$) interactions, the cross sections are identical to the muon neutrino (antineutrino) nucleon cross sections. Because of the rapid energy loss or annihilation of electrons and positrons, it is generally true that only contained-vertex events can be observed. Since electron neutrino fluxes are small, an extremely large effective volume is needed to get measurable event rates. There is one exceptional case: resonant formation of W^- in $\bar{\nu}_e e$ interactions at $E_\nu = 6.3 \text{ PeV}$. The resonant cross section is larger than the νN cross section at any energy up to 10^{21} eV . In Fig. 4 we present neutrino-electron cross sections.

We note that, at the resonance energy, upward-moving electron antineutrinos do not survive passage through the Earth. However, the contained events have better prospects for detection. The contained event rate for resonant W production is

$$\text{Rate} = \frac{10}{18} V_{\text{eff}} N_A \int dE_{\bar{\nu}_e} \sigma_{\bar{\nu}_e e}(E_{\bar{\nu}_e}) S(E_{\bar{\nu}_e}) \frac{dN_{\bar{\nu}_e}}{dE_{\bar{\nu}_e}}. \quad (9)$$

We show event rates for resonant W -boson production in Table 3. The background is for events with $E_\nu > 3 \text{ PeV}$.

From Table 3 we note that a 1 km^3 detector with energy threshold in the PeV range would be suitable for detecting resonant $\bar{\nu}_e e \rightarrow W$ events. However, the $\nu_\mu N$

Figure 4: Cross sections for neutrino interactions on electron targets. At low energies, from largest to smallest cross section, the processes are (i) $\bar{\nu}_e e \rightarrow$ hadrons, (ii) $\nu_\mu e \rightarrow \mu \nu_e$, (iii) $\nu_e e \rightarrow \nu_e e$, (iv) $\bar{\nu}_e e \rightarrow \bar{\nu}_e e$, (v) $\bar{\nu}_e e \rightarrow \bar{\nu}_e e$, (vi) $\nu_\mu e \rightarrow \nu_\mu e$, (vii) $\bar{\nu}_\mu e \rightarrow \bar{\nu}_\mu e$.

background may be difficult to overcome. By placing the detector a few km underground, one can reduce atmospheric-muon background, which is 5 events per year per steradian at the surface of the Earth for $E_\mu > 3$ PeV.

SUMMARY

In summary, we find that detectors such as DUMAND II, AMANDA, BAIKAL and NESTOR have a very good chance of being able to test different models for neutrino production in the AGNs.²⁴ For $E_\mu^{\min} = 1$ TeV, we find that the range of theoretical fluxes leads to event rates of 900-29,600 upward-moving muons/yr/km²/sr originating from the diffuse AGN neutrinos, with the atmospheric background of 1400 events/yr/km²/sr. For $E_\mu^{\min} = 10$ TeV, signal to background ratio becomes even better, with signals being on the order of 500-8,400 events/yr/km²/sr, a factor ~ 20 -300 higher than the background rate. For neutrino energies above 3 PeV there is significant contribution to the muon rate due to the $\bar{\nu}_e$ interaction with electrons, due to the W -resonance contribution. We find that acoustic detectors with 3 PeV threshold and with effective volume of 0.2 km³, such as DUMAND, would detect 48 hadronic cascades per year from $W \rightarrow$ hadrons, 7 events from $W \rightarrow \mu \bar{\nu}_\mu$ and 36 events from ν_μ and $\bar{\nu}_\mu$ interactions with virtually no background from ATM neutrinos.

Acknowledgements

This work was supported in part by DOE grants DE-FG03-93ER40792, DE-FG02-85ER40213, and NSF Grant PHY 95-07688. Fermilab is operated by Universities Research Association, Inc., under contract DE-AC02-76CHO3000 with the United States Department of Energy.

REFERENCES

1. C. E. Fichtel, *et al.*, *Astrophys. J. Suppl.* 94:551 (1994).
2. M. Punch, *et al.* (Whipple Observatory Gamma Ray Collaboration) *Nature (London)* 160:477 (1992); A.D. Kerrick *et al.*, *Astrophys. J.* 438:L59 (1995); J. Quinn, *et al.* (Whipple Observatory Gamma Ray Collaboration) *IAU Circular* 6169 (June 16, 1995).
3. T. C. Weekes, private communication.
4. See T. Gaisser, F. Halzen and T. Stanev, *Physics Reports* 258:173 (1995) for a review of neutrino astronomy and sources of UHE neutrinos.
5. J. Babson *et al.*, (DUMAND Collaboration), *Phys. Rev.* D42:3613 (1990); *Proceedings of the NESTOR workshop at Pylos, Greece*, ed. L. K. Resvanis (University of Athens, 1993); D. Lowder *et al.*, *Nature* 353:331 (1991).
6. R. Gandhi, C. Quigg, M.H. Reno and I. Sarcevic, hep-ph/9512364, to appear in *As-troparticle Physics* (1996).
7. ZEUS Collaboration, M. Derrick *et al.*, *Phys. Lett.* B316:412 (1993); H1 Collaboration, I. Abt *et al.*, *Nucl. Phys.* B407:515 (1993).
8. C. Quigg, M. H. Reno and T. Walker, *Phys. Rev. Lett.* 57:774 (1986); M. H. Reno and C. Quigg, *Phys. Rev.* D37:657 (1988).
9. L. V. Volkova, *Yad. Fiz.* 31:1510 (1980) (*Sov. J. Nucl. Phys.* 31:784 (1980)).
10. L. Nellen, K. Mannheim and P. L. Biermann, *Phys. Rev.* D47:5270 (1993).
11. A. P. Szabo and R. J. Protheroe, *Astropart. Phys.* 2:375 (1994).
12. F. W. Stecker, C. Done, M. H. Salamon and P. Sommers, *Phys. Rev. Lett.* 66:2697 (1991); Errat.: *Phys. Rev. Lett.* 69:2738 (1992). Revised estimates of the neutrino flux appear in F. W. Stecker and M. H. Salamon, astro-ph/9501064, submitted to *Space Sci. Rev.*
13. S. Yoshida and M. Teshima, *Prog. Theoret. Phys.* (Kyoto) 89:833 (1993).
14. W. H. Rhode *et al.* (Fréjus Collaboration), Wuppertal preprint WUB-95-26, to appear in *Astropart. Phys.*
15. P. Gondolo, G. Ingelman and M. Thunman, Uppsala preprint TSL/ISV-95-0120, hep-ph/9505417.
16. S. R. Mishra, *et al.* (CCFR Collaboration), Nevis Laboratory Report Nevis-1465 (1992), and in *Lepton-Hadron Scattering*, Proceedings of the Nineteenth SLAC Summer Institute on Particle Physics, edited by Jane Hawthorne, SLAC-REPORT-398 (1992), p. 407.
17. Rolf Beyer, 1995 *Workshop on Weak Interactions and Neutrinos*, Talloires, France.
18. V.N. Gribov and L.N. Lipatov, *Sov. J. Nucl. Phys.* 15:438 (1972); L.N. Lipatov, *Sov. J. Nucl. Phys.* 20:181 (1974); Yu.L. Dokshitser, *Sov. Phys. JETP* 46:641 (1977); G. Altarelli and G. Parisi, *Nucl. Phys.* B126:298 (1977).
19. E.A. Kuraev, L.N. Lipatov and V.S. Fadin, *Sov. Phys. JETP* 44:443 (1976); 45:199 (1977); Ya.Ya. Balitskii and L.N. Lipatov, *Sov. J. Nucl. Phys.* 28:822 (1978).
20. A.D. Martin, W.J. Stirling and R.G. Roberts, *Phys. Rev.* D47:867 (1993); *Phys. Lett.* 354B:155 (1995).
21. H. Lai *et al.*, *Phys. Rev.* D51:4763 (1995).
22. L. V. Gribov, E. M. Levin and M. G. Ryskin, *Phys. Rep.* 100:1 (1983). See also D. W. McKay and J. P. Ralston, *Phys. Lett.* 167B:103 (1986).
23. E. Eichten, I. Hinchliffe, K. Lane and C. Quigg, *Rev. Mod. Phys.* 56:579 (1984); *ibid.* 58:1065E (1986).

24. See §7 of T. K. Gaisser, F. Halzen and T. Stanev, Ref. 4, for a review of several models in addition to the models presented here.
25. A. Dziewonski, "Earth Structure, Global," in *The Encyclopedia of Solid Earth Geophysics*, ed. D. E. James (Van Nostrand Reinhold, New York, 1989), p. 331.
26. P. Lipari and T. Stanev, *Phys. Rev.* D44:3543 (1991).

